- Technical Paper -

PRE- AND POST-YIELDING TENSILE BEHAVIORS OF R/HPFRCC

Mahyarudin DALIMUNTHE[*1], Benny SURYANTO[*2], and Kohei NAGAI[*3]

ABSTRACT

This paper investigates the response of reinforced HPFRCC in tension. 1,700-mm long specimens reinforced with 0.7, 1.7, and 3% of rebar were tested. Test results show that, except in specimen with 0.7% rebar, which failed due to rebar pull-out, the HPFRCC was capable to deform compatibly with the rebar prior to yielding. This is confirmed by uniform steel strain profile, formation of multiple cracks along the specimens, and steel response similar to bare bar. Crack localizations were observed at the post-yielding stage. A comparison the tensile response of R/HPFRCC and RC is presented.

Keywords: reinforced HPFRCC, pull out, compatible deformation, crack localization

1. INTRODUCTION

Previous research has shown that HPFRCC exhibits remarkable tensile characteristics, including small crack width and outstanding tensile ductility. Despite this remarkable tensile property, the use of rebar is generally required when it is used as structural members. To predict the behavior of the member accurately, it is important to understand the tensile characteristics of reinforced HPFRCC (R/HPFRCC).

On characterizing the tensile behavior of R/HPFRCC, previous research was conducted based on the results of short specimens of about 500 mm or less [1]. As such, the effects of boundary conditions can be of significant to the results. Hence it is difficult to obtain the true behavior of HPFRCC. Fantili *et al* identified this issue and tried to enlarge the cross section of the rebar near both ends of their specimens with two additional short rebars [2]. They demonstrated that the proposed method was effective to decrease the occurring end slips at both specimen ends and hence more reliable HPFRCC response could be extracted.

In this study, R/HPFRCC specimens with length of 1.7 meter are used to eliminate the boundary effects. Attention is focused on the response of both rebar and HPFRCC in the pre- and post-yielding stages and failure modes. Focus is also made to the formation and number of localized cracks, if such crack exists during loading. In the last part of this paper, the average response of R/HPFRCC is compared with RC, focusing on the behavior of the rebar and HPFRCC. Based on two different rebar models, the average tensile stress of HPFRCC in R/HPFRCC is discussed.

2. TEST PROGRAMS

2.1 Materials

The HPFRCC material used in this study is a premix type of Engineering Cementious Composite (ECC) that contains of Polyvinyl Alcohol (PVA) fibers. The mixture proportion of the ECC is shown in Table 1.

Table 1 Mix Proportion of PVA-ECC

W/(C+FA) (%)	Water (kg/m^3)	S/(C+FA) (%)	PVA Fibers (%), in vol.
42.2	350	70	2.0

Note: W: Water, C: Cement, FA: Fly Ash, S: Sand. PVA fibers: diameter is 0.04 mm, length is 12 mm, and tensile strength is 1,600 MPa.

2.2 Description of the Test Specimens

Three specimens with a square cross-sectional area of 130x130 mm^2 and length of 1,700 mm were prepared (see Fig. 1). A single screw shaped rebar was used in each specimen. The diameter of the rebar was varied among 13 mm, 19 mm, and 25 mm, corresponding to a reinforcement ratio of 0.7%, 1.7%, and 3.0% respectively. To ensure the rebar inside the specimen yields before the rebar outside the specimen, a higher strength of rebar was used outside. A coupler was used to connect both types of rebar at each specimen end. The rebar properties are summarize in Table 2.

Table 2 Reinforcement Property

Dia. (mm)	Normal Strength f_y (MPa)	High Strength f_y (MPa)	H (mm)	P (mm)
13	340	430	1.00	7
19	384	685	1.75	8
25	384	685	2.00	10

Note:

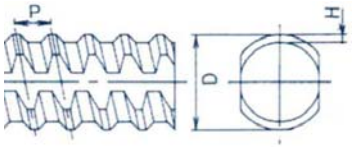

*1 Graduate Student, Dept. of Civil Engineering, University of Tokyo, JCI Member
*2 Postdoctoral Research Fellow, Dept. of Civil Engineering, University of Tokyo, JCI Member
*3 Lecturer, Dept. of Civil Engineering, University of Tokyo, JCI Member

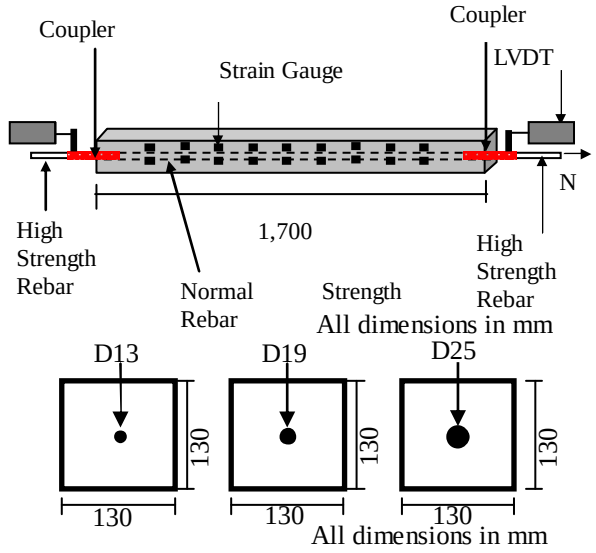

a) Specimen Descriptions

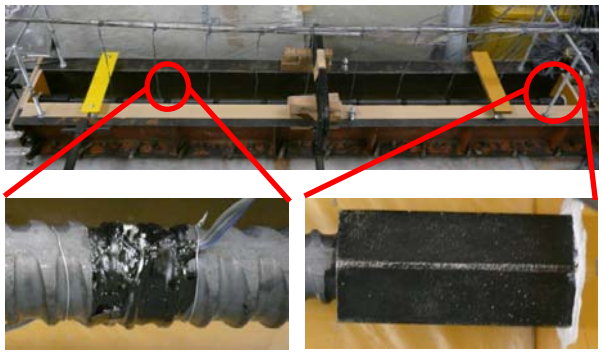

b) Framework and Detail of the Reinforcement

Fig. 1 Tensile Test Setup

2.3 Casting and Curing Condition

The specimens were cast in a horizontal position perpendicular to the loading direction. After casting, all specimens were put in a controlled room with 20°C temperature and 60% humidity condition until 28 days and covered with plastic sheets. After one day, the specimens were demolded and covered with wet burlaps and plastic sheets. Three cylinders with 100-mm diameter and 200-mm height were prepared and tested after 28 days. The results are shown in Table 3.

To obtain the tensile ECC property, dog bone shaped specimens with cross sectional area of 60x60 mm^2 were made. The specimens were tested under direct tension with a fixed boundary condition at both ends. The results are depicted in Figure 2 and summarized in Table 3.

Table 3 Mechanical Properties of the ECC

ECC	Value
$f'c$ (MPa)	37.47
ε_c (%)	0.47
f_{cr} (MPa)	2.07
f_{tu} (MPa)	2.7
ε_{tu} (%)	0.5

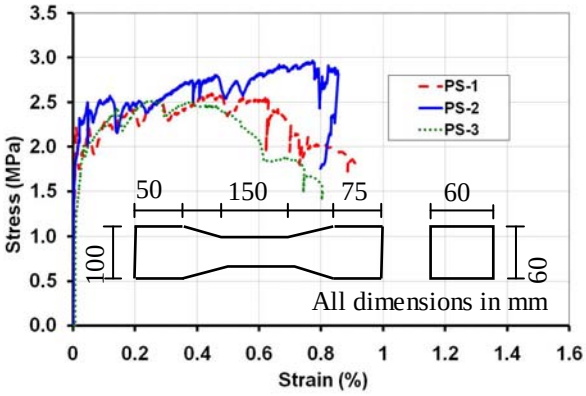

Fig. 2 ECC Tensile Test Response

2.3 Test Setup

Figure 3 illustrates the geometry and instrumentation for conducted experiment. A rectangular steel frame was used for the tensile test. Each specimen was put at the centre of the frame, resting on six roller supports. The support was used to eliminate friction between the specimen and the floor (see Fig. 3).

A 500 kN hydraulic jack was used for applying the tensile load. The load was applied to the reinforcement at one side of the specimen. On the other side, the reinforcement was bolted to the frame to provide a reaction force to the applied tension force.

Two LVDTs were used for measuring the average strain for every loading step. The LVDTs were used to measure the displacement difference of the two couplers attached on each end side of the specimens. In order to obtain local steel strain information, 18 strain gauges were attached on the rebar inside the specimen at an interval of 150 mm from the centre of the specimens to both sides (for clarity, see the illustration depicted in Fig. 1(a)).

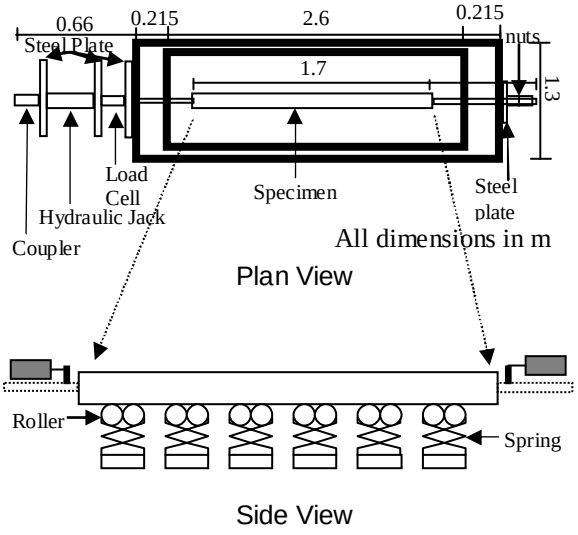

Fig.3 Experimental Setup

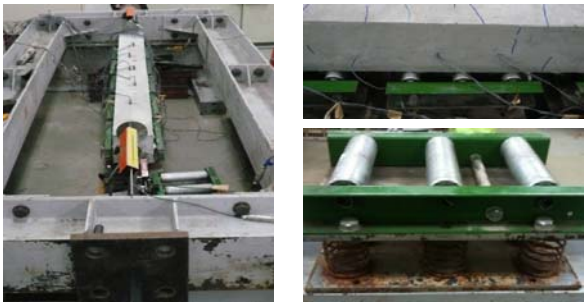

Details of Roller Supports
Fig.3 Experimental Setup (continued)

3. TEST RESULTS

3.1 Stress Strain Behavior

The load-deformation response of the R/ECC for the three specimens is depicted in Figure 4 by plotting the applied load versus the average strain of the R/ECC. These responses are compared with bare bar stress strain behavior.

Figure 4(a) shows the load deformation response of PL-1 specimen with reinforcement ratio (ρ) 0.7%. The load was interrupted when it reached 7, 25, and 45 kN, marked by letter A to C in the figure for crack observation. The maximum load reached 57 kN (point D), when the overall strain reached 0.13%. Loading was stopped when the rebar inside the specimen had already pulled out about 4 cm without any sign of crack localization in the ECC. Until the load stopped, there was no crack localization formed.

For PL-2 specimen (ρ 1.7%), the loading was interrupted at 20, 50, 75, and 100 kN, marked by letter A to D in Figure 4(b). The load was also interrupted when the average strain reached 0.6% (point F) due to sudden increase of crack width at about the center of the specimen. The maximum load was 131 kN occurring at the average strain of 0.3%. The first and the second crack localization (see Fig. 5b) occurred almost simultaneously at the average strain of about 0.4% (Point E). As soon as crack localization occurred, the load gradually decreased up to 0.5% average strain. After that, the load increased gradually. At Point G, the load was unloaded to observe the width of the crack localization. The load was continued until the average strain reached 1.6%. The loading was stopped due to large crack opening of the crack localization at about the centre of the specimen. There were two crack localizations when the load was terminated.

Results of specimen PL-3 (ρ 3.0%) are depicted in Figure 4(c). The loading was interrupted at 50, 100, and 170 kN, as marked by letter A to C in the figure. The rebar inside ECC started to yield when the load reached almost 200 kN. At the first yielding, the length of the specimen increased (Point D). That is, the load was about constant and the strain increased suddenly. After that, the load increased again. After reaching 210 kN, the load decreased gradually and the first crack localization formed (Point E). This crack occurred when the average strain reached 0.4%. As in the PL-2, the first crack localization also occurred in the centre of the specimen (see Fig. 5(c)). The load then increased again in which the inclination is almost linear. The second and the third crack localization occurred almost simultaneously when the average strain reached 1.2% (see letter F in Fig. 4). The fourth and fifth crack localizations formed when the average strain reached 1.7%, and were located between the previous cracks (see Fig. 5(c)). The loading was stopped due to large crack opening at the first crack localization. Five crack localizations formed in PL-3 specimen when the load was terminated. Compared to the crack localization of the previous two specimens, it appears that the number of crack localization is influenced by the reinforcement ratio. The number of the crack localizations increases as the reinforcement ratio increases.

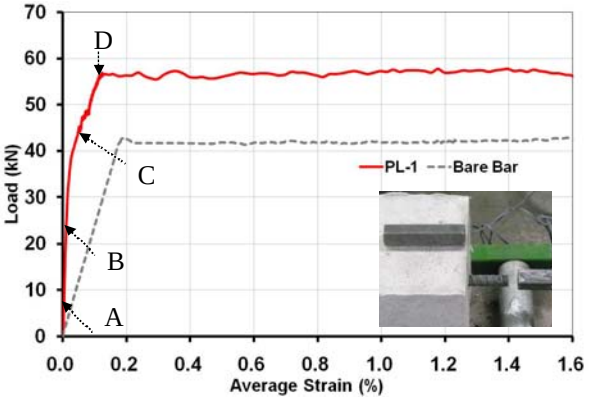

a) Tensile Load of PL-1

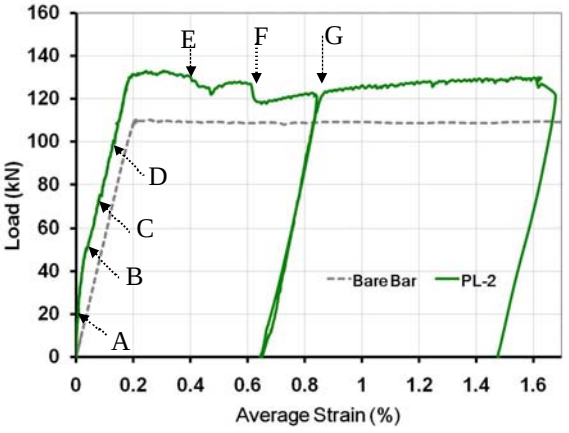

b) Tensile Load of PL-2

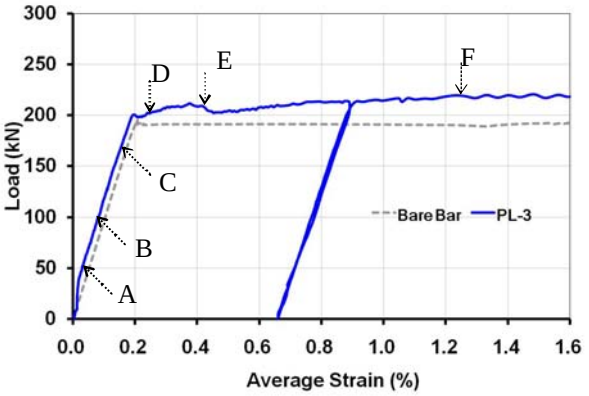

c) Tensile Load of PL-3
Fig. 4 Tensile Load of Specimens

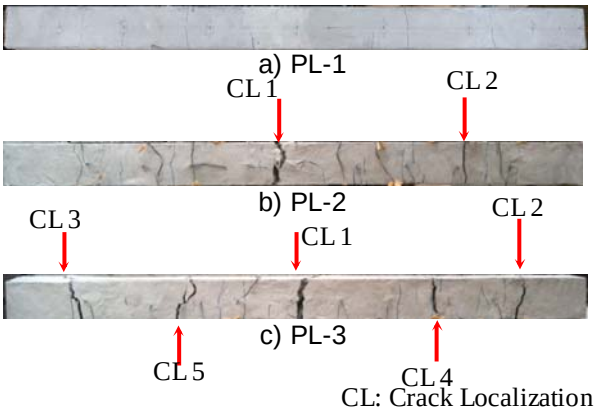

CL: Crack Localization

Fig. 5 Crack Pattern of the Specimens after Test

3.2 Local Strain Values

Figure 6 to 8 shows the profile of local steel strain of each specimen for various load levels prior to the yielding. For specimen PL-1, the local steel strains along the specimen vary. At beginning of load level, the steel strain distribution along the specimen almost uniform. At 40 kN, the difference in local steel strain started. The reason of having such a difference is not clearly understood. A possible explanation is that a local slip may occur due to the limited size of the ribs in 13-mm diameter rebar. In specimens PL-2 and PL-3, the distribution of the steel strains is almost uniform for every load level. This demonstrates that the deformation between the ECC and the rebar is compatible (see Fig. 7 and 8).

Figures 9 and 10 show the local steel strain profile of specimens PL-2 and PL-3 in the post yield region at selected load levels. Higher steel strain was observed in the area where the crack localization occurred. In specimen PL-2, the highest steel strain was obtained at the strain gauges 60 mm from the first crack localization (noted as Point A) and 40 mm from the second crack localization (noted as Point B). At Point A, the local steel strain reached 1.3%, occurring when the average strain reached 0.7%, while at Point B the local strain reached 1.1% at average strain of 1.6%. The local steel strain at point A decreased when the steel strain at Point B started to increase towards its maximum value.

In specimen PL-3, the highest local steel strain was obtained at the strain gauges located at 50, 40, and 30 mm from the first, the forth, and the fifth crack localizations. As shown in Figure 10, the local steel strain at Point A reached 0.7%, 1.15% at Point B, and 0.7% at Point C. These strains occurred at the average strain of 0.44% and 1.7%, respectively. These three steel strain values occurred at different load levels, occurring almost coincidentally with the relevant crack localization. Unfortunately, the local steel strain near the second and the third crack localizations could not be obtained since the locations were about 73 mm and 63 mm from the second and the third crack localizations to the nearest strain gauges.

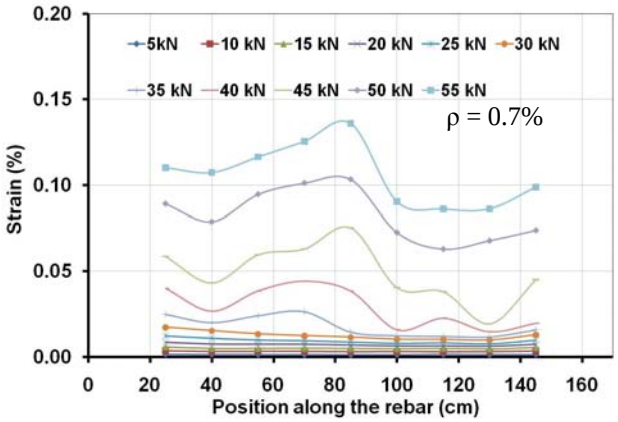

Fig. 6 PL-1 Steel Strain Responses (Pre-yielding)

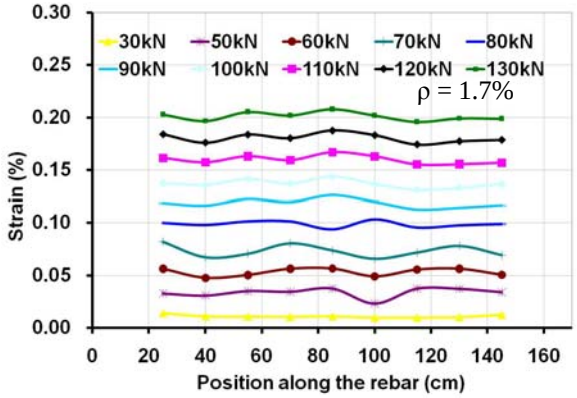

Fig. 7 PL-2 Steel strain Response (Pre-yielding)

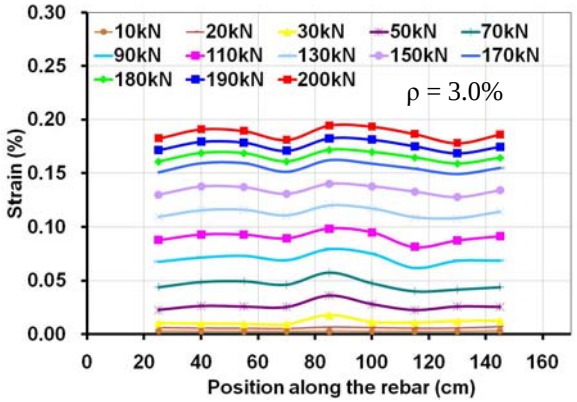

Fig. 8 PL-3 Steel Strain Response (Pre-yielding)

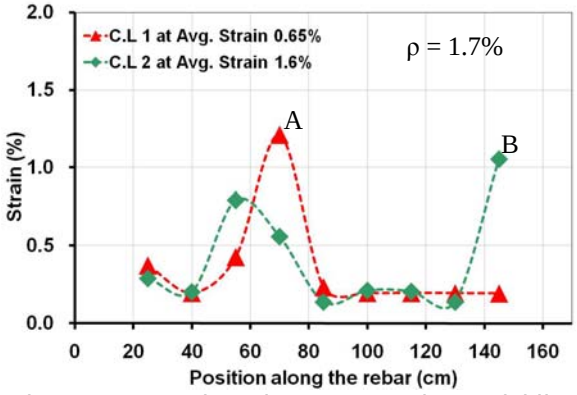

Fig. 9 PL-2 Steel Strain Response (Post-yielding)

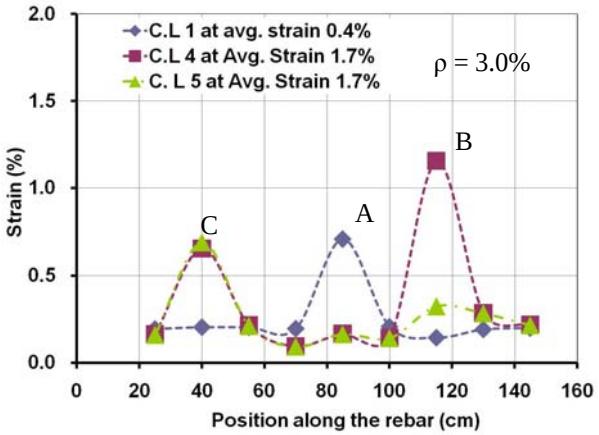

Fig. 10 PL-3 Steel Strain Response (Post-yielding)

3.3 Crack Observation

To observed the internal crack pattern of R/ECC, the specimens were cut along their longitudinal direction about 90 cm length or 45 cm from center to both end sides by using concrete cutting machine as depicted in Figure 11. The internal crack pattern observed using black light. The cutting surface was painted with fluorescent paint powder. The crack observation results are shown in Figure 12.

Figure 12 (a) shows the crack pattern in PL-1 (0.7%). It shows that crack was formed along the rebar between ECC and rebar which made the rebar pull out during tested.

Figure 12 (b) and (c) are the crack observation results of PL-2 (1.7%) and PL-3(3.0%) specimens. There are two different types crack pattern formed in these specimens. First pattern is orthogonal crack pattern (picture 1) and second is conical shape crack pattern (picture 2). From the observation shows that first pattern formed in area with small crack localization width while second pattern was formed in large width of crack localization.

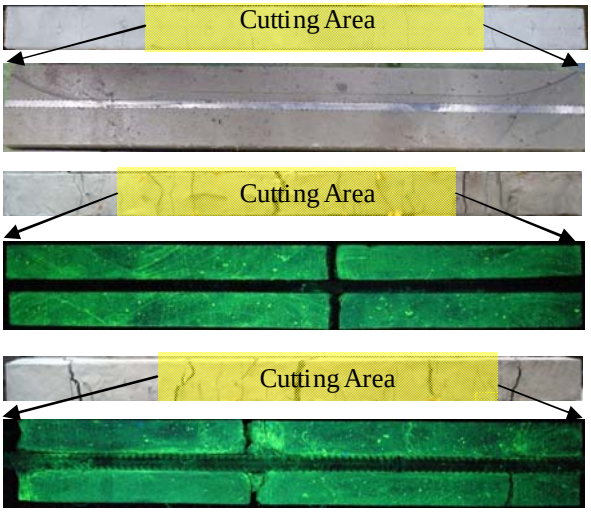

Fig. 11 Cutting Specimens

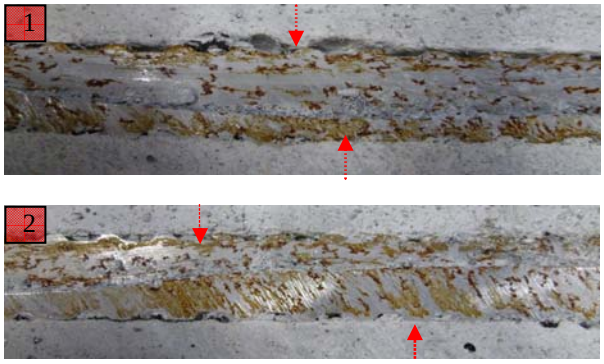

a)Crack Pattern of PL-1

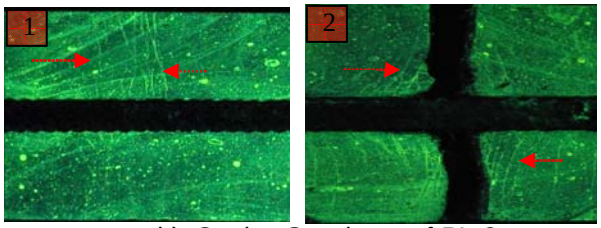

b) Cutting Specimen of PL-2

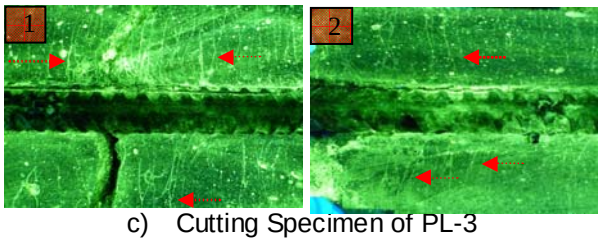

c) Cutting Specimen of PL-3

Fig. 12 Internal crack observation results

4. DISCUSSIONS

4.1 Average Tensile Response of R/ECC and R/C

A comparison is made between tensile response of R/ECC and RC. The responses of R/ECC are based on test results of PL-2 (1.7%) and PL-3 (3.0%). The response of RC is computed based on the summation of the tri-curved steel model [3], a model of rebar in concrete, and the tension stiffening concrete model proposed by Okamura and Maekawa [3].

Figures 13 and 14 show that R/ECC have a better tensile performance than RC, especially in the pre-yielding region. The yielding point in the R/ECC is similar to that of bare bar at a strain of approximately 0.2%. This is in contrast to the yielding occurrence in RC, which is always less than 0.2%, as a result of local steel stress increases at cracks. This demonstrates the contribution of fibers in the ECC. Even after yielding, the R/ECC still exhibits a better tensile performance.

After crack localizations formed in the R/ECC, it appears that contribution of the ECC decreases, but is still higher than that of concrete. Interestingly, both R/ECC (after crack localization) and RC exhibit similar slope of load increase, indicating that segments of rebar at the localized cracks in the R/ECC reached strain-hardening. The higher tensile load in the R/ECC can be explained by the fact that number of crack localization in R/ECC is much less than that in RC and hence the average tensile stress of the ECC is higher.

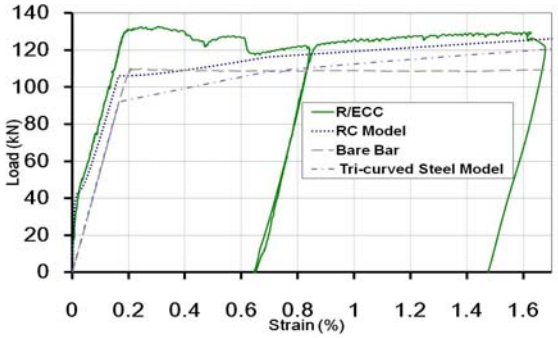

Fig. 13 PL-2 and RC Macroscopic Response

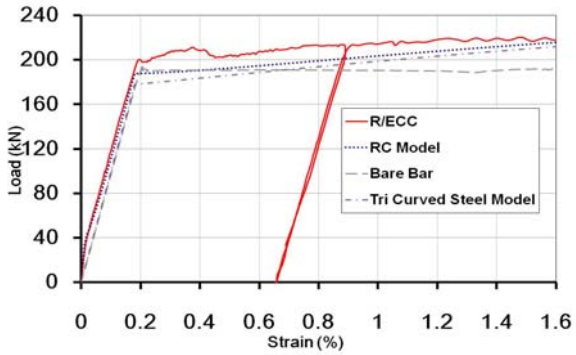

Fig. 14 PL-3 and RC Macroscopic Response

4.2 ECC Response on R/ECC

To shed light on the average response of ECC in R/ECC, the total tensile load of the R/ECC is subtracted with the rebar load and then divided with net cross-sectional area of the ECC. Two tentative models are assumed for defining the rebar response in R/ECC: 1) bare bar model, and 2) bare bar model with the value of the strain hardening starts from the value computed from the tri-curved steel model [3]. Note that since the average strain measured in the two specimens was less than the strain hardening strain of the rebar (about 1.8%), Model 1 is essentially an elastic-plastic model.

Figure 15 presents the average stress-strain of ECC in R/ECC based on the two rebar models, with the ECC stress values are normalized with respect to the first cracking tensile stress of the ECC. It is clear that the response of the ECC fluctuates almost at a constant stress, an indication of multiple cracking, until the average strain of about 0.2%, which is the yielding of the rebar. From average strain of 0.2% to 0.4% (initiation of crack localization), the ECC stress is almost constant and about 20% less. From 0.4% to about 0.68% (average strain hardening strain assumed), the ECC still exhibits significant tensile stress.

From average strains of about 0.68%, the ECC stress computed from both rebar models deviate each other. Model 1 tends to overestimate the ECC tensile stress, since the model fails to consider the strain-hardening of rebar segments at cracks. In contrast, Model 2 tends to underestimate the ECC response, since the number of crack localization observed in R/ECC is, in fact, less than that generally observed in RC. Thus, it is believed that the average tensile stress-strain of ECC during this stage is in between the values computed based on the two rebar models used and is under of current investigations.

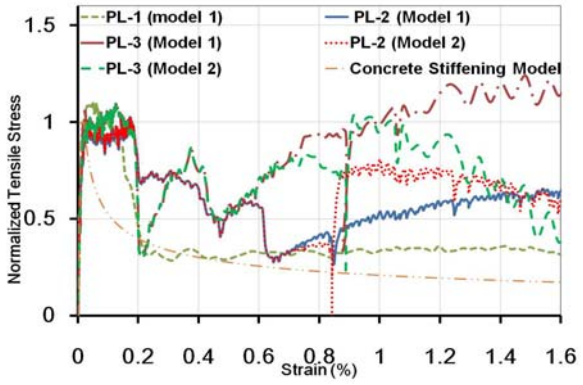

Fig. 15 ECC Response in R/ECC

5. CONCLUSIONS

(1) The ability of ECC to carry tensile force together with rebar is confirmed in the test specimens with reinforcement ratio of 1.7% and 3.0% during pre-and post-yielding stages.

(2) The test specimen reinforced with 0.7%, the rebar failed due to the progressive pull-out failure from one end. This failure occurs possibly due to smaller rib height and spacing of the rebar.

(3) In other specimens, both ECC and rebar can deform compatibly during the pre-yielding stage. This is confirmed by a uniform strain profile along the specimens and multiple cracks orthogonal to the longitudinal direction of the specimens.

(4) Crack localizations were observed at the post-yielding stage. The R/ECC still can carry tensile forces due to bond between the two.

(5) The number of the crack localization appears to be influenced by reinforcement ratio. Two crack localizations were observed in the test specimen reinforced with 1.7%, and five in that with 3.0%. The multiple cracks nearby the crack localizations were in a conical shape.

(6) The response of rebar in R/ECC has the same response with bare bar prior to the formation of localized cracks. Afterwards, R/ECC behaves similar to RC. Macroscopic load increases due to strain hardening of rebar at the localized cracks.

REFERENCES

[1] Li,V.C. and Fischer, G., “Influence of Matrix Ductility on Tension-Stiffening Behavior of Steel Reinforced Engineering Cementious Composites (ECC)”, ACI Structural Journal, Vol. 99, No.1, 2002, pp. 104-111.

[2] Fantilli, A.P., Mihashi, H., and Vallini, P., “Strain compatibility between HPFRCC and steel reinforcement,”, Vol. 38, No. 4, 2005, pp. 495-503.

[3] Maekawa, K., Pimanmas, A., Okamura, H.,”Nonlinear Mechanics of Reinforced Concrete”, Spon Press, 2003, pp.632-637